submitted to the Astronomical Journal, 5 October 2002

Direct measurement of the size of the large Kuiper belt object () Quaoar

Michael E. Brown & Chad Trujillo
Division of Geological and Planetary Sciences, California Institute of Technology,
Pasadena, CA 91125

ABSTRACT

We imaged the recently discovered bright Kuiper belt object () Quaoar[1] with the Hubble Space Telescope High Resolution Camera to directly determine its size. The PSF of each of 16 images was carefully measured from a field star 13 arcseconds from Quaoar, and the expected PSF at the location of Quaoar was convolved with Quaoar's motion vector and a model resolved disk. A least-squares analysis was performed to find the best-fit disk size. The apparent diameter of Quaoar was resolved as 40.4 ± 1.8 milliarcseconds. Accounting for the uncertainty due to an unknown limb darkening function, the size of Quaoar is 1260 ± 190 km with a red and blue albedos of $0.092^{+0.036}_{-0.023}$ and $0.101^{+0.039}_{-0.024}$, respectively. These albedos are significantly higher than the canonically assumed value of 4%. Quaoar is the largest currently known minor planet.

1. Introduction

Many hundreds of Kuiper belt objects (KBOs) are currently known, and an understanding of their history, dynamics, and surface properties is gradually emerging. The sizes of KBOs are, however, almost entirely unknown. To date, only two of the largest objects have had their sizes reliably measured. These measurements have used the technique of radiometry, wherein a temperature for the object is assumed from the heliocentric distance and a measurement of thermal emission is then converted to an emitting area and therefore object size. Emission at a wavelength of 0.85 mm has been detected from (20000)

[1]Note to the editor: By the time of publication, this object, which currently has a provisional designation 2002 LM60, will be officially numbered and named and we will replace the name given here. We have proposed the name "Quaoar" and expect that it will be accepted.

Varuna (Jewitt, Aussel, & Evans 2001) and at 1.3 mm from 2002 AW197 (Margot et al. 2002) at fluxes of $2.81 \pm .85$ and 1.05 ± 0.30 mJy, respectively, implying sizes of 900^{+124}_{-145} and 890^{+115}_{-130} km. The R-band albedos implied from these measurements combined with the optical fluxes of the objects are $0.07^{+.03}_{-.02}$ and $0.10^{+0.04}_{-0.02}$, respectively, higher than the canonical 4% value assumed for KBOs in most studies. Some of the largest errors in these analyses are the systematic errors – unaccounted for in the above error bars – associated with understanding the thermal emission of the object.

The discovery of the extremely bright KBO () Quaoar presented the opportunity to attempt the measurement of the size of a KBO in a direct and entirely different manner. At a magnitude of $R = 18.5$, a geocentric distance of 43.4 AU, and an assumed albedo of 4%, Quaoar's diameter would be 1910 km, almost as large as that of Pluto. Even assuming a higher albedo of 10%, Quaoar would be 1210 km, about half the size of Pluto and larger than its moon Charon. Objects of these sizes at the distance of Quaoar should be directly resolvable with the Hubble Space Telescope (HST). At a wavelength of 435 nm, the High Resolution Camera (HRC) has a resolution of 40 milliarcseconds (mas), corresponding to 1250 km at the distance of Quaoar. With careful PSF measurement, objects with diameters ever smaller than this resolution are resolvable. We thus undertook HRC observations of Quaoar to determine the size of this potentially large KBO and to provide an alternative method for the size measurement of the largest KBOs.

2. Observations

We obtained 16 120-second exposures of Quaoar using the High Resolution Camera (HRC) of the Advanced Camera for Surveys (ACS) in the F435W filter on 1 August 2002 in one orbit of the Hubble Space Telescope (HST). The observations began 4:50 on 29 July 2002 and one observation was obtained every 171 seconds. The timing of the observations was chosen so that Quaoar would be a few arcseconds from a moderately bright field star, and the telescope was tracked at the sidereal rate so that accurate PSF measurements could be obtained. The motion of Quaoar caused a smearing of about 60 mas of the image of Quaoar during each 120-second observation, a factor which needed to be taken carefully into account in the analysis of the size.

The star had a brightness of 32650 ± 170 counts ($B = 18.47 \pm 0.01$) in each of the images and was single, well exposed, and not saturated. Quaoar had a brightness of 9920 ± 50 counts ($B = 19.76 \pm 0.01$) and traveled across a field uncontaminated by detectable background stars or galaxies in the stacked images. These fluxes were determined from our full PSF fitting analysis, described below.

3. PSF determination

3.1. Field star PSF

Determination of the angular size of Quaoar is dependent on an accurate measurement of the PSF of the field star. This measurement is complicated by two factors. First, at a wavelength of 435 nm, the HRC PSF is undersampled. With a FWHM of 40 and a pixel size of ∼25 mas, the core of the PSF changes noticeably depending on the precise sub-pixel position of a source, so direct measurement of the stellar PSF and translation to Quaoar at different sub-pixel positions would be imprecise. Second, the HRC images onto a distorted field on which the distortion changes with field position. Thus even if a precise PSF could be measured at the position of the field star, the PSF would differ at the location of Quaoar. The change of the PSF over the 13 arcsecond distance from the field star to Quaoar is likely small, nonetheless a reliable measurement of the angular size of Quaoar needs to take even this small variation into account.

To accommodate the difficulties of PSF measurement with the HRC, we used the PSF simulation software TinyTim[2] to help measure the PSF of the field star for each image (Krist & Hook 2001). TinyTim simulates PSFs of HST images through direct computation of the diffraction pattern caused by passage through the entire optical system. The HRC is a new instrument on HST and the current version of TinyTim (6.0) uses only a pre-flight ray trace of the instrument, thus needs to be extensively validated before modeled PSFs are used. Examination of the field star images demonstrated that the PSF of HST during these observations was time variable. The HST suffers from a well known temporal focus shift, known as "breathing" induced by thermal expansion and contraction of the secondary support structure. Accurate characterization of these shifts and any other shifting aberrations was also critical to precise PSF modeling.

Initial tests with TinyTim showed that focus shifts over the one orbit of observation are the single largest contributors to PSF change. The total focus change corresponds to about 7 μm of secondary shift. In addition, it was clear from the residuals of data minus model that significant and relatively constant trefoil (known as "clover" in TinyTim) was present in the image PSFs and that varying degrees of astigmatism and coma also occurred in the images. We therefore concluded that the proper procedure was to perform a least-squares fit for the first 8 relevant Zernike terms in each image (defocus, 2 astigmatisms, 2 comae, 2 trefoils, and spherical aberration) using the field star.

---

[2]TinyTim is available at http://www.stsci.edu/software/tinytim

The full procedure to create a best-fit TinyTim model of the PSF on one image proceeded as follows. First, TinyTim was used to generate a five-times super-sampled geometrically distorted PSF at the location of the field star using nominal parameters for the first 8 Zernike terms. This PSF was resampled with varying sub-pixel centering and convolved with the appropriate CCD charge diffusion kernel. A least-squares minimization between the model and the data was then performed to find the best-fit sub-pixel centering and total flux value for the nominal PSF. The TinyTim parameters were then modified by hand to create new PSFs with the Zernike terms varied one-by-one from defocus to spherical aberration, solving for a best-fit sub-pixel center and total flux for each new PSF. At each step, a least-squares optimal magnitude of the Zernike term was found until all 8 terms were determined. The process is CPU intensive and involves testing of many varying PSF models, but the process is simplified by the fact that the Zernike polynomials are orthonormal so that fitting of each term is independent of the others (a fact that we empirically verified after-the-fact by testing small variations in all parameters). Figure 1 shows the Zernike terms of the best fit model determined from the field star for all 16 images. The defocus smoothly varies from 5 μm out of focus to 2μm past optimal focus, a typical behavior owing to breathing of the telescope secondary. In addition, the astigmatism, coma, and spherical aberration vary in concert with the focus. Of all terms, only trefoil appears to be constant. This large relatively static trefoil term causes the largest deviation from the data PSF of any term other than defocus.

The final match between the data and the PSF model is excellent. Figure 2 shows one of the 16 stellar images along with the final TinyTim model and the residuals. In this case, the residuals are indistinguishable from Poisson plus readout noise. In other cases, higher order aberrations occur at extremely low levels, but, as we will later demonstrate, these residuals are sufficiently small as to not affect our measurement of the angular size of Quaoar.

3.2. Modeled PSF verification

No model of a real PSF will perfectly represent the true PSF, thus a test to determine if imperfections in our modeled PSF can mimic in any way a resolved object is crucial. Our original choice of 8 Zernike terms to model was based in part on the hope that by including all terms up to the first two spherically symmetric terms (defocus and spherical aberration) any remaining aberrations in the PSF would not mimic a resolved object. We tested that hypothesis by attempting to measure the size of the star in each of the 16 images (which should be a point source) using the method that we will use to measure

the size of Quaoar. We describe this method in detail below, but in Fig. 3 we show the measured angular size of the star in each image to demonstrate that in 10 out of 16 cases the star is indistinguishable from a point source convolved with the derived model PSF. In the remaining cases, the measured size of the PSF is either 13 or 14 mas, which are our first two measurable sizes above a point source. We thus conclude that in at least 10 cases, our PSF models are sufficiently well-matched to the data that they do not introduce any artificial apparent size to point sources and that any size we measure in these 10 images of Quaoar is indeed intrinsic to the source. The 6 images with slightly worse PSF fits were discarded from further analysis, though it is shown below that their inclusion does not affect the final result.

3.3. Field dependent distortion verification

Accurate knowledge of the PSF at the position of Quaoar requires that we trust that if TinyTim produces a PSF which matches the field star, it will also produce a PSF which matches Quaoar 13 arcseconds away. To test if this ability is indeed the case, we examined HRC F435W images of 47 Tuc obtained in April 2002 for flat-field stability calibration purposes. We use our method described above to model the PSF of a star at the same position of our field star and to model the PSF of a star at the position of Quaoar. The parameters obtained for the Zernike terms are indistinguishable, suggesting that TinyTim's pre-flight incorporation of field distortion provides an excellent model for HRC distortions over these small distances. As a further check, we used the PSF model produced for the location of the field star, created a PSF at the location of Quaoar with the same parameters, and attempted to measure the angular size of a star at the location of Quaoar. We again find that the star at the location of Quaoar is indistinguishable from a point source. These tests lend confidence to our ability to determine the PSF at the location of our field star and trust the subsequent PSF model at the location of Quaoar.

4. The size of Quaoar

For each image we now have an accurate model of the PSF at the position of Quaoar. Theoretically we could deconvolve the data with this PSF to determine the size and motion of Quaoar, but without significantly more sampling of the data such a deconvolution will not provide reliable results. We chose instead to determine the size of Quaoar by forward modeling the effects of observing a resolved disk with the PSF determined at the position of Quaoar.

The first step was to determine the motion of Quaoar in each image. Quaoar moves along a curved path resulting from a combination of orbital motion, terrestrial parallax, and HST parallax. The x and y centroid positions as functions of time were fit to third-order polynomials to smoothly define the motion of Quaoar. The amount of motion during each observation was determined by the derived difference in position at the beginning and end of each observation. The mean motion in the distorted image plane in the x direction is 0.90 pixels during one observation, while the mean motion in y is 2.2 pixels.

We then modeled each image as a geometrically distorted convolution of the model PSF and a model disk convolved with the motion vector. We used as the non-distorted model PSF the intermediate TinyTim output of the model PSF at a pixel scale of 12.1 mas per pixel. A model disk of diameter d was then created by resampling a 100 by 100 image of a Lambert sphere (different potential limb darkening functions for the disk are discussed below) by a factor of $100/d$ to the super-sampled pixel scale. The model PSF was then convolved with this model disk to create the modeled images of a non-geometrically distorted non-moving disk. This model disk image was then geometrically distorted by TinyTim to create a 5 times super-sampled model image of a non-moving disk, and finally this model image was convolved with the measured motion vector to create a super-sampled geometrically distorted appropriately moving model image of a disk of diameter d. As above for the PSF stars, the super-sampled model image was then resampled to the image pixel scale with various sub-pixel center positions and convolved with the CCD charge transfer kernel, and a least-squares minimization was performed to find the best sub-pixel x and y center of the image and total flux of the image. The entire procedure was repeated while varying the diameter d of the model disk until the minimum least-squares best value of d was obtained for each of the 16 images.

The model image fits to the data are generally excellent with the exception of one image which suffered a cosmic-ray hit near the core of the PSF and was therefore not included in further analysis. Fig. 4 shows a typical image of Quaoar compared with the modeled image and residuals.

The best fit values for d are shown in Fig. 3. The mean of the 9 reliable measurements is 3.34 super-sampled 12.1 mas pixels with a standard deviation of 0.43 mas for a best fit angular size of 40.4 ± 1.8 mas. At a distance of 42.9 AU this size corresponds to a diameter of 1260 ± 55km. If the 5 rejected images for which a finite size for the PSF star was measured are included, the final size is only 30 km smaller, suggesting that the small PSF mismatches that led us to reject these images actually have little effect on the final answer.

The small scatter in these 9 independent measurements is a testament to the accuracy of the PSF models created from extensive TinyTim modeling of the field star. Confidence

that this level of accuracy is warranted comes from the work of Noll et al. (1995) who performed similar measurements of the size of the near-earth asteroid (4179) Toutatis. The angular size of Toutatis was similar to the size measured for Quaoar, and the HST measurements were consistent with independent radiometric measurements.

5. Systematic sources of error

The measurement of the size of Quaoar is remarkably precise; the random error bars of 4% are significantly smaller than those of 15% obtained for (2000) Varuna (Jewitt, Aussel & Evans 2001) and 13% obtained for 2002 AW197 (Margot et al. 2002) using thermal radiometry. The main sources of error in the size of Quaoar, however, are likely to be systematic rather than random.

One potentially large source of systematic error is the unknown limb darkening function of Quaoar. For our initial measurement we assumed that the disk of Quaoar reflected as a Lambert surface and therefore had a limb darkening function of $I = \cos^2 \alpha$, where I is the brightness of a surface element at angle α from the sub-solar point (assumed to be the same as the sub-observer point). For a Lambertian sphere with diameter d, half of the total light falls within a diameter of $0.6d$. Experimentation with other limb darkening functions suggestions that these functions will change the derived size approximately proportionately to the change in half-total light diameter. For example, if Quaoar has a limb darkening function closer to lunar, the half-total light diameter would be approximately $0.7d$ and the true size of Quaoar would be 1090 km. If Quaoar instead has a surface with a strong specular reflection it could have a much smaller half-total light diameter, and actually be larger. The true limb darkening function of such an icy outer solar system body is unknown. We take as representative errors the range from the Lambert to lunar limb darkening function and estimate an error for this unknown of 15%.

Another potential source of error could be a non-spherical shape or non-uniform surface of Quaoar. In our analysis we have assumed that Quaoar is a round and featureless body. Lightcurve measurements show, however, that Quaoar has a 20% intensity variation over a period of many hours (Trujillo & Brown, in preparation). Such a variation could be due either to surface features or to a non-spherical shape, though a body of this size with a moderate rotation rate would be expected to be spherical. We nonetheless consider both effects.

First we model an ellipsoid with axes in the ratio of 1.2:1.0 and fit a circular model. We find that the best-fit circular model has a diameter of the geometric mean of the two axes,

thus the model provides accurate results about the surface area viewed. We next model two extreme cases of surface spots. First we create a model sphere having a single small area with twice the normal albedo and 0.44 the diameter of the disk at the sub-observer point which would cause a 20% flux variation. We then attempt to model this object as a uniform sphere. The derived size is again approximately proportional to the half-total light diameter, such that the modeled size is ∼10% smaller than the true size. If instead this bright spot is placed 60 degrees from the observer on the limb the modeled size is only ∼2% larger than the true size. Larger numbers of albedo spots will tend to make the disk more uniform and will cause fewer problems. We thus estimate that this effect causes an uncertainty of 10% in the final size derivation.

A final source of error, and the only observational process that we could not adequately test with our analysis of the 47 Tuc observations, is any effect caused by the motion of Quaoar over the individual exposures. Errors in the motion vector with which we convolve our model could cause inaccuracies in our final measurements. These motion vectors are accurately defined by fitting to the full motion of Quaoar over the full orbit, nonetheless we explore the effects of these errors. If we rerun the entire analysis but introduce 10% random x and y offsets to the modeled motion vector of each image, we find the the final angular size measured is unchanged, though the scatter is slightly larger. We thus conclude that this final potential systematic error has no discernible effect on the derived angular size.

6. Conclusion

Our final estimate of the diameter of Quaoar is 1260 ± 190 km, with the error bars dominated by the systematic error of the unknown limb darkening profile. The red albedo, based on an opposition red magnitude of 18.5 ± 0.1 (with the uncertainty due to the unknown phase of the light curve at the time of observations) is $0.092^{+0.036}_{-0.023}$ while the blue albedo, based on a measured blue magnitude of 19.76 ± 0.01 and assuming an opposition brightening of 0.15 mag deg^{-1} is $0.101^{+0.039}_{-0.024}$.

The red albedo is consistent with the two values measured for other KBOs from radiometry. Assuming the albedos of all 3 objects are identical (which is not known to be the case, but is a plausible hypothesis), we infer an average albedo of $0.088^{+0.021}_{-0.012}$. This albedo is significantly larger than the canonical 4% that is assumed in many studies. It is not known if most other KBOs have this albedo or if these largest KBOs, which are the only ones currently measured, are different. In addition, these 3 measured KBOs are all members of the high inclination hot classical population population of the Kuiper belt (Brown 2000; Morbidelli & Brown 2003) whose members are distinguishable in color

(Trujillo & Brown 2001) and possibly also maximum size (Levison & Stern 2001, Morbidelli & Brown 2003) from the low inclination cold classical population, so their albedo properties might also be expected to be different. Assuming this albedo hold for large objects, the 4 intrinsically brightest KBOs – Quaoar, 2002 AW197, Ixion, and Varuna – have diameters of 1290, 960, 960, and 800 km, respectively. Quaoar would thus be the largest known minor planet and the largest object found in the solar system since the discovery of Pluto. While our current understanding of the albedos and sizes of KBOs is highly biased, continued application of this technique and the technique of millimeter radiometry, and the future use of SIRTF thermal measurements will soon begin to provide the first hints of any interesting population properties of sizes and albedos of the objects in the Kuiper belt.

Acknowledgement: We would like to thank the director and staff at STScI for providing the opportunity to make these measurements and the assistance in making them happen. In particular, without prodding from Ian Griffin we would not have taken this second set of data which allowed us to shrink the random error bars by a factor of 6.

REFERENCES

Brown, M.E. 2001, AJ, 121, 2804

Margot, J.-L., Trujillo, C., Brown, M.E., & Bertoldi, F. 2002, BAAS, in press

Jewitt, D., Aussel, H., & Evans, A. 2001, Nature, 411, 446

Krist, J. & Hook, R. 2001, The Tiny Tim User's Guide Version 6.0

Levison, H.F. & Stern, S.A. 2001, AJ, 121, 1730

Morbidelli, A. & Brown, M.E. 2003, in Comets II, eds. Festou, M., Keller, H.U., & Weaver, H.A., submitted.

Noll, K.S., Weaver, H.A., Storrs, A.D,, Zellner, B. 1995, Icarus, 113, 353.

Trujillo, C.A. & Brown, M.E. 2002, ApJ, L125

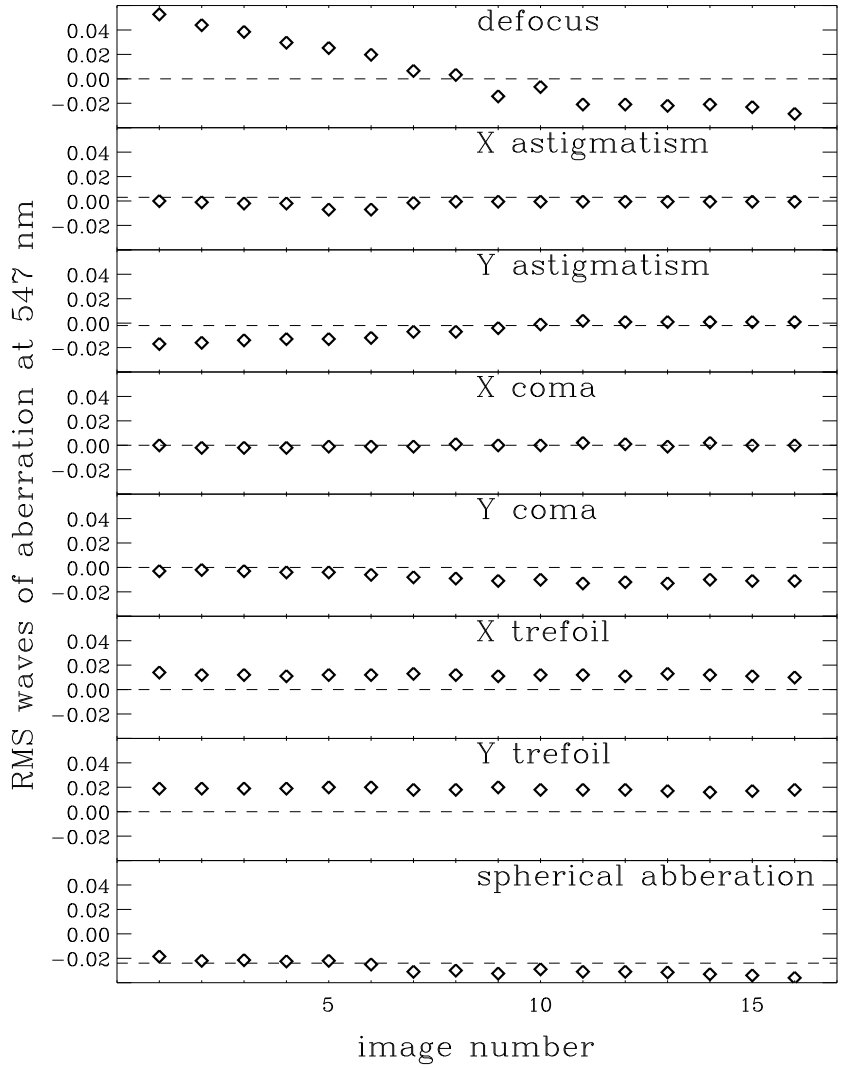

Fig. 1.— Magnitude of the Zernike terms determined from the field star in each image, in units of RMS waves of aberration at 547 nm. The dashed line shows the nominal TinyTim expected value for each term. For defocus, 0.011 waves of aberration correspond to 1 μm of secondary focus shift. The smooth change in defocus over the orbit of observation is consistent with the well known temperature induced secondary position changes ("breathing") of the HST. Coma, astigmatism, and spherical aberration shift in concert with focus. Trefoil, which causes the largest PSF mismatch of any term other than defocus, is large and constant throughout the observations.

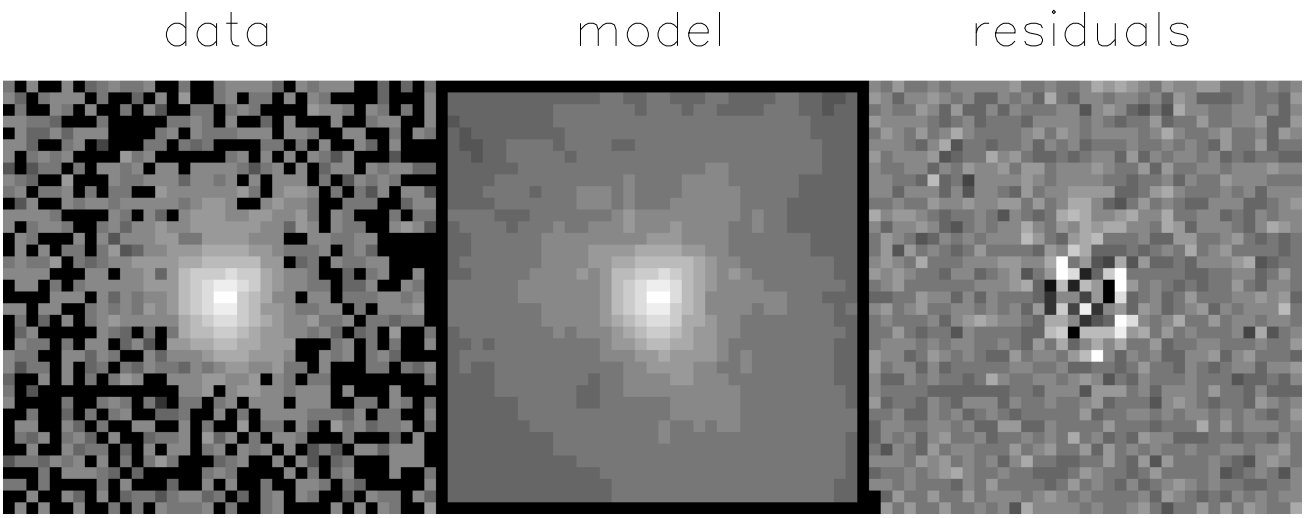

Fig. 2.— Comparison of one of 16 images of the field star, the best-fit TinyTim PSF, and the residuals. The data and model share the same logarithmic scale. The residuals are linearly scaled from ±1% of the maximum of the model image. The residuals are consistent with read plus Poisson noise.

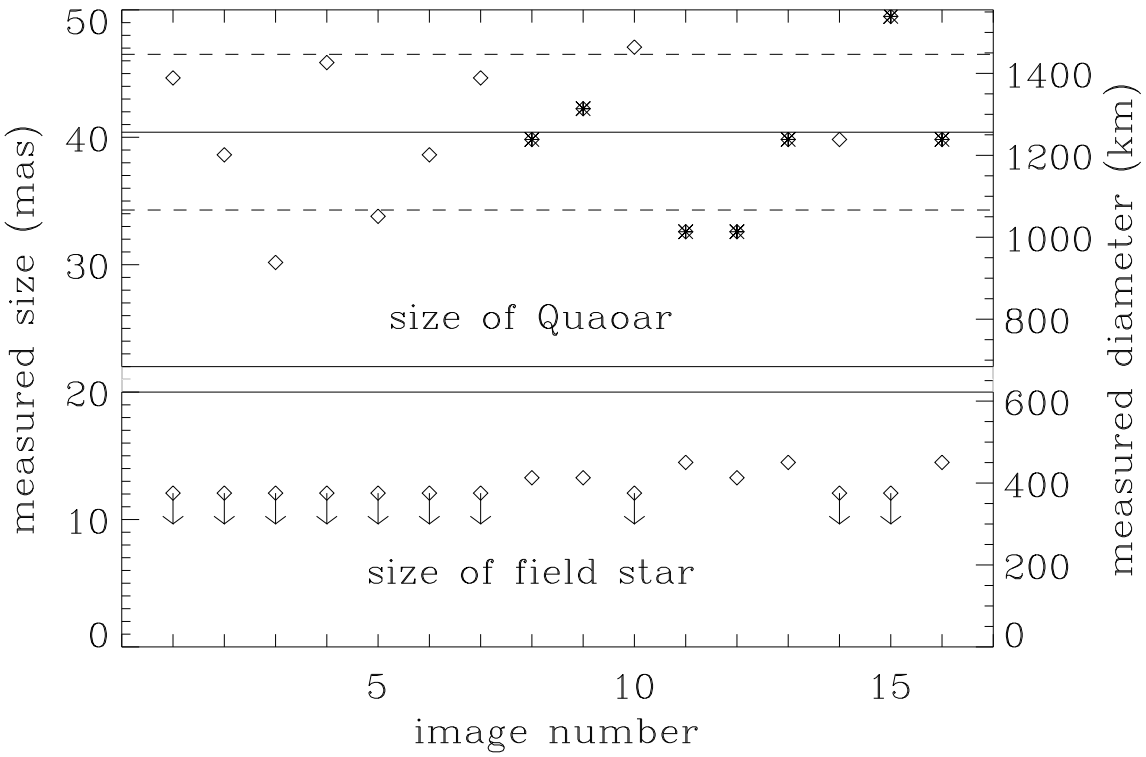

Fig. 3.— Angular size and linear size measured for the field star and for Quaoar in the 16 images. The six images for which we measured a finite size for the star (8, 9, 11, 12, 13, 16) and the one image for which we find a cosmic ray hit near the center of Quaoar (15) are marked and not used for further analysis, though their inclusion does not affect the final results. For the remaining 10 images, the average size of Quaoar is 40.4 ± 1.8 mas, or 1260±55 km. Taking into account systematic effects, the true errors are larger, leading to a result of 1260±190 km, which is shown by the range of the dashed lines.

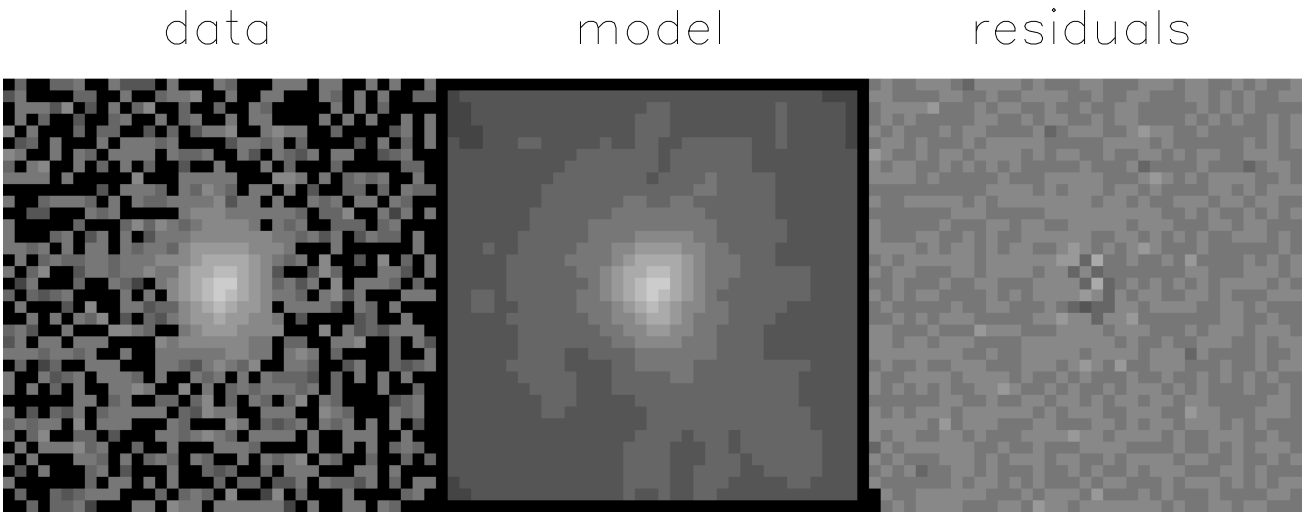

Fig. 4.— Comparison of one of 16 images of Quaoar, the best-fit model of a moving Quaoar of size 39 mas, and the residuals. The data and models share identical logarithmic scales. The residuals are linearly scaled from ±1% of the maximum of the model image.